Journal of Sea Research 212 (2026) 102718

Contents lists available at ScienceDirect

Journal of Sea Research

journal homepage: www.elsevier.com/locate/seares

Seagrass habitat mapping using UAV imagery in a port environment in Sabah, Malaysia

Pei Zhao Liew, Imelus Nius, Ashley Loduni, Wei Sheng Chong *

Borneo Marine Research Institute, Universiti Malaysia Sabah, Kota Kinabalu, Malaysia

ARTICLE INFO

Keywords:
Unmanned aerial vehicle (UAV)
Drone
Benthic habitat mapping
Port environment
Coastal monitoring
Malaysia

ABSTRACT

Seagrass habitats in port environments are exposed to high anthropogenic pressure; however, baseline spatial information is often limited at the site scale required for environmental assessment and monitoring. This study mapped benthic habitats in a working port using ultra-high-resolution unmanned aerial vehicle (UAV) imagery and in situ reference observations. UAV images were processed into a georeferenced orthomosaic at 1.31 cm per pixel, covering 9.364 ha. Object-based image analysis and supervised classification were used to map six benthic habitat classes: seagrass, mixed seagrass, coral, coral rubble and coarse sand, fine sand, and deep water. Fine sand was the dominant class (3.819 ha; 41%), followed by coral rubble and coarse sand (3.597 ha; 39%). Seagrass habitats covered 0.522 ha (~6%), comprising 0.304 ha of dense seagrass meadows dominated by *Enhalus acoroides* and 0.218 ha of mixed seagrass assemblages dominated by *Cymodocea serrulata* and *Halophila ovalis*. Accuracy assessment yielded an overall accuracy of 88.71%, with high chance-corrected agreement (Kappa = 0.843; Tau = 0.865). Misclassifications were concentrated in the vegetated transition zones and along boundaries with unconsolidated substrates. The results demonstrate that UAV-based mapping can provide a repeatable baseline for port-scale habitat assessment and targeted monitoring, while remaining sensitive to depth, water clarity, and sun glint conditions.

1. Introduction

Seagrasses are marine flowering angiosperms that grow in shallow coastal waters and require sufficient light for survival (Lin et al., 2021). Seagrass meadows provide multiple ecosystem services, including shoreline protection through wave attenuation and sediment stabilisation (Bremner et al., 2023). Their belowground structures bind sediments and reduce wave-induced sediment resuspension (Christianen et al., 2013). Seagrass habitats also support coastal biodiversity by providing nursery and refuge areas for fish and invertebrates and contribute to improved coastal environmental quality (Fortes et al., 2018).

The spatial trajectory of these ecosystems varies significantly across global, regional, and local scales. While cumulative impacts from climate-induced anomalies and coastal development historically precipitated widespread global declines (Tan et al., 2020), recent multi-decadal assessments indicate that decline is no longer a universal trajectory for all seagrass populations (de los Santos et al., 2019; Orth and Heck Jr, 2023). In several areas with stringent environmental regulations, notable trend reversals and population recoveries have occurred; for instance, European meadows have shown structural improvements in area and density since the 2000s following strict nutrient input controls (de los Santos et al., 2019), and fishery-stressed meadows have successfully re-established following targeted improvements in urban wastewater infrastructure (Román et al., 2024). In contrast to these managed recoveries, seagrass ecosystems in the highly biodiverse waters of Southeast Asia and the Coral Triangle face persistent, acute threats from ongoing coastal conversion (Kamal et al., 2023). Within Malaysia, which hosts 18 distinct seagrass species, long-term monitoring datasets and multi-decadal records reveal a dominant trend of habitat fragmentation and localized loss rather than recovery (Kamal et al., 2023; Zakaria et al., 2025a; Zakaria et al., 2025b). Intensive regional pressures—such as industrial port expansion, nearshore land reclamation, and capital dredging—have driven immediate habitat removal and severe water-column turbidity from chronic sediment resuspension (Zakaria et al., 2025b). Furthermore, recent temporal observations in pressured Malaysian waters reveal troubling structural transformations, characterized by the displacement of stable climax species by transient

* Corresponding author.
E-mail address: chong@ums.edu.my (W.S. Chong).

https://doi.org/10.1016/j.seares.2026.102718
Received 7 February 2026; Received in revised form 5 June 2026; Accepted 10 June 2026
Available online 12 June 2026
1385-1101/© 2026 The Author(s). Published by Elsevier B.V. This is an open access article under the CC BY-NC-ND license (http://creativecommons.org/licenses/by-nc-nd/4.0/).

macroalgae or sparse, highly vulnerable species like *Halophila beccarii* (Zakaria et al., 2025a; Zakaria et al., 2025b). Given that localized losses sharply diminish coastal economic and ecological value, generating rapid centimetre-scale spatial baselines in high-exposure industrial zones has become an operational prerequisite for adaptive coastal management.

Sabah and Southeast Asia are important regions for seagrass biodiversity and distribution; however, knowledge of seagrass and baseline mapping remain limited for many local sites (Freeman et al., 2008). This creates a severe management gap, particularly because empirical valuations highlight that Malaysian seagrass meadows provide critical socioeconomic services, including gleaning, artisanal fisheries support, and downstream economic value, worth an estimated US$57,732 (RM242,474) ha^{-1} $year^{-1}$ (Rahman and Yaakub, 2020). Despite these high baseline values, sensitive nearshore meadows are heavily exposed to the accelerating expansion of maritime infrastructure. Sabah Port, located in Sepanggar Bay, is a major industrial and logistics area that serves as a gateway for goods entering and leaving Sabah and supports intensive port infrastructure and cargo operations.

According to official throughput records from Sabah Ports Sdn Bhd, the total container traffic across the state reached a record of 532,391 twenty-foot equivalent units (TEUs) in 2025 (up from 386,293 TEUs in 2024). This expansion was heavily concentrated within the immediate study site, where the Sapangar Bay Container Port underwent a dramatic 60.8% operational surge, increasing its specific handling volume from 246,798 TEUs in 2024 to 396,964 TEUs in 2025 following management integration with Dubai Port World (DPW) - Sabah.

The bay is approximately 20 km from Kota Kinabalu, and the coastal zone around the sampling site is surrounded by industrial areas, ports, and buildings. Deep-water berths allow large container vessels to dock in port systems. Seagrass occurrence has previously been reported in the coastal area around Sabah Port (Bujang et al., 2006), and the seagrass habitat contributes to shoreline stabilisation and supports coastal harvesting (gleaning) activities (Bujang et al., 2006). However, a precise baseline seagrass map has not been established for this specific site, despite the immediate presence of nearshore seagrass patches threatened by this escalating industrial and maritime footprint.

Remote sensing is widely used for mapping seagrass habitats because it provides spatially continuous observations that are less time-consuming than field surveys (Hossain et al., 2015; Makri et al., 2023). Satellite imagery enables repeatable, broad-scale mapping; however, its effectiveness in shallow coastal waters can be limited by spatial resolution, water depth, water clarity, and surface reflectance effects (Hossain et al., 2015; Wicaksono and Lazuardi, 2021). Field-based approaches, such as snorkelling, diving, and transect or quadrat surveys, provide detailed habitat information but are labour-intensive and spatially limited (Bremner et al., 2023; Freeman et al., 2008; Koedsin et al., 2016; Muhamad et al., 2021; Rajamani and Marsh, 2015). In heterogeneous nearshore environments, these constraints create a practical gap between the spatial detail needed for site-level management and the information typically available for baseline assessment and monitoring of these habitats.

Unmanned aerial vehicles (UAVs) offer a complementary remote sensing platform capable of acquiring centimetre-scale imagery over targeted coastal areas with flexible acquisition timing (Duffy et al., 2018; Ventura et al., 2018). UAV-based mapping can reduce cloud constraints and resolve small habitat patches and fine boundary structures that are often unresolved in medium-resolution satellite products (Bremner et al., 2023; Greene et al., 2018; Tahara et al., 2022).

However, the operational deployment of UAV methodologies introduces distinct socioeconomic and technical challenges that are frequently overlooked by researchers. Although consumer-grade RGB drone hardware is substantially more affordable than commercial satellite tasking or manned aircraft missions, establishing an operational mapping pipeline still requires notable economic investments. These costs include specialized photogrammetric structure-from-motion (SfM) software, advanced object-based image analysis (OBIA) licenses, and recurring civil aviation regulatory processing fees necessary to secure legal flight authorisations in industrial zones. Beyond financial constraints, a major bottleneck is the limited institutional availability of trained personnel equipped with the interdisciplinary skill set required to navigate flight planning, regulatory compliance, photogrammetric reconstruction, and machine learning classification workflows. In heterogeneous nearshore environments, these technical and economic constraints create a practical gap between the spatial detail needed for site-level management and the information typically available for baseline assessment and monitoring of these resources.

To date, the deployment of UAV workflows for seagrass assessment has primarily focused on ecologically pristine, stable, and highly accessible systems. These include shallow, clear-water coral reef lagoons in the Western Indian Ocean (Hamad et al., 2022), protected estuarine borders utilising multispectral sensors (Duffy et al., 2018), low-energy tropical lagoon meadows (Bremner et al., 2023), and macro-tidal intertidal flats where meadows emerge completely at low tide to circumvent water column interference entirely (Trinh et al., 2023). However, substantial uncertainties remain regarding the performance of these drone workflows in heavily modified, optically complex industrial landscapes, such as busy shipping ports. Port environments present unique challenges for optical remote sensing, including severe depth-gradient transitions from dredged berths to nearshore zones, high localized wave action from commercial vessels, and complicated benthic backgrounds containing mixed industrial debris, coarse coral rubble and shifting sands. Consequently, it remains unclear whether standard consumer-grade red-green-blue (RGB) UAV sensors can reliably decouple highly fragmented mixed-species seagrass patches (*Enhalus acoroides*, *Cymodocea serrulata*, and *Halophila ovalis*) from surrounding sediment classes under high-pressure industrial conditions without requiring specialized multispectral equipment or exhaustive water column correction models.

This study provides a site-scale baseline map of seagrass and associated benthic habitats in a port environment using UAV imagery supported by in situ reference observations. The outputs quantify habitat composition and spatial configuration in a development-pressured coastal setting and establish a repeatable reference layer for regional monitoring and impact assessment in the future. The workflow is intended for operational use in shallow nearshore waters, where field surveys alone are spatially limited and medium-resolution satellite products may not resolve fragmented habitats.

2. Methods

An overview of the methodology, including in situ data collection, UAV image acquisition, orthomosaic generation, object-based image analysis, supervised classification, and accuracy assessment, is presented in Fig. 1.

2.1. Study area and overall workflow

The study was conducted at Sabah Port, Sepanggar Bay, Sabah, Malaysia (hereinafter referred to as Sabah Port), which is situated approximately 20 km north of Kota Kinabalu along the northwest coast of Borneo (Fig. 2). The survey footprint covered a nearshore maritime corridor of 9.364 ha, adjacent to active commercial container berths and port logistics infrastructure.

As the primary maritime gateway for the state of Sabah, this port handles the vast majority of the state's containerised cargo and industrial trade. According to official maritime traffic statistics from Sabah Ports Sdn Bhd, total container throughput across all state ports reached a record 532,391 TEUs (twenty-foot equivalent units) in 2025. This logistics traffic is heavily centralized within our immediate study area; the Sapangar Bay Container Port underwent a significant 60.8% operational cargo handling surge, jumping from 246,798 TEUs in 2024 to 396,964

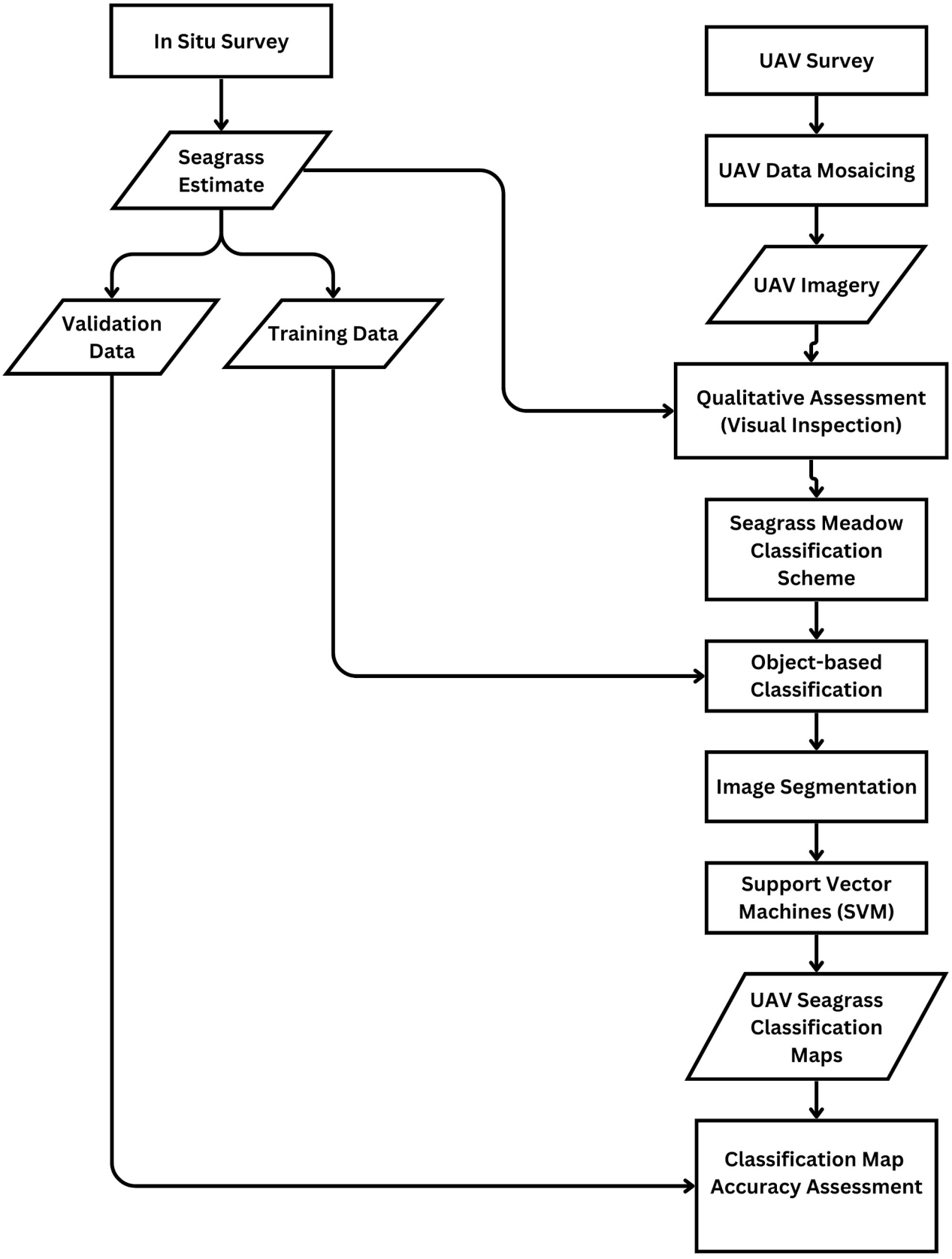

Fig. 1. Workflow for UAV-based seagrass habitat mapping at Sabah Port, Sepanggar Bay, Malaysia.

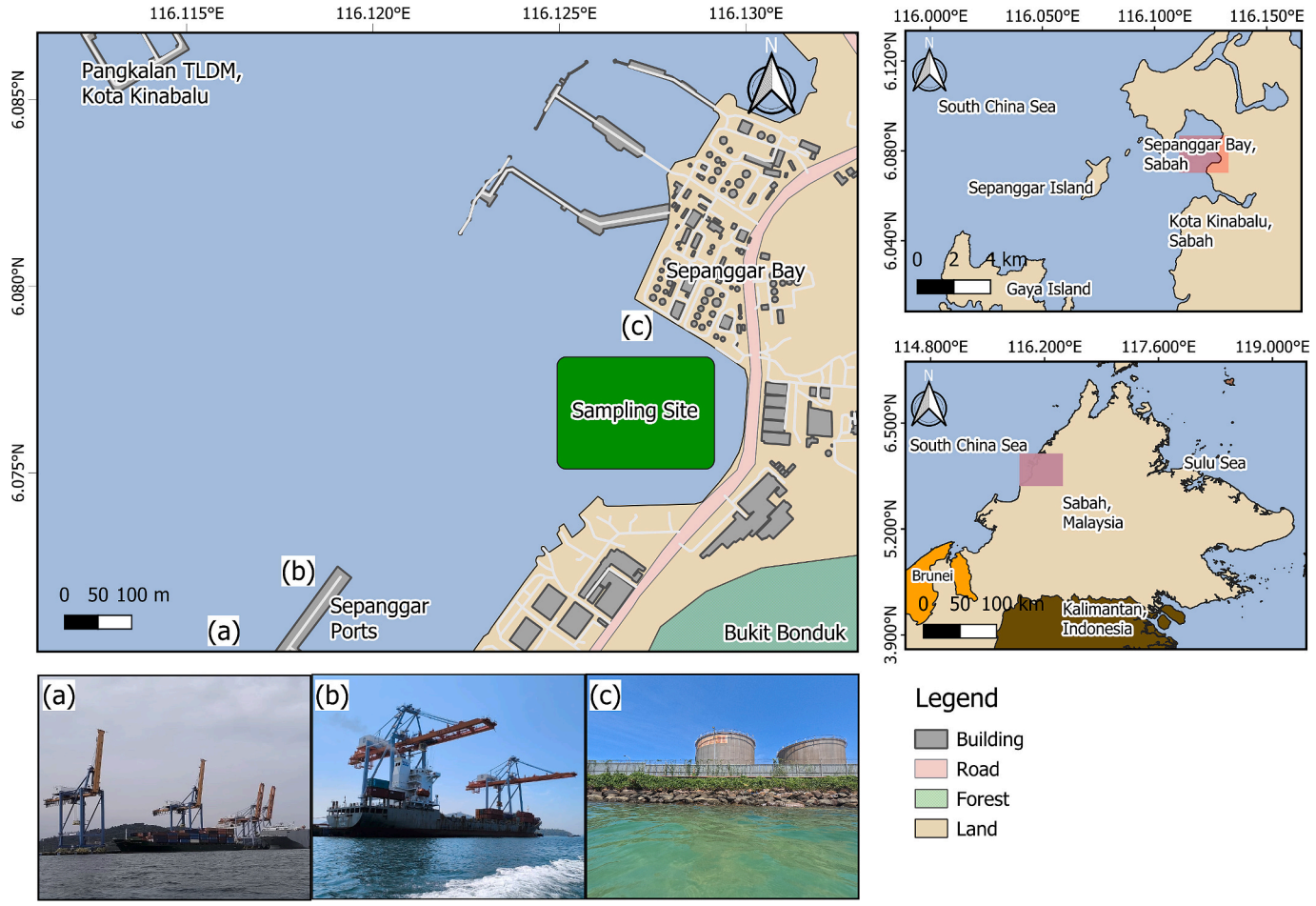

Fig. 2. Location of the study area at Sabah Port.

TEUs in 2025 under its unified management framework with DP World - Sabah.

The coastal zone around the sampling site is surrounded by dense industrial zones, terminal facilities, and administrative buildings. Deep-water berths within the port system allow large container vessels to dock close to the shoreline, creating a steep depth-gradient transition from the dredged channels to the shallow intertidal flats. The climate is equatorial with two major monsoonal periods: the Northeast Monsoon (November to March) and the Southwest Monsoon (May to September).

Both UAV and in-situ surveys were conducted during low tide (0.8–0.9 m relative to mean sea level) to increase seabed visibility and reduce water column effects on optical imagery. UAV image acquisition was carried out on 20 September 2024. In-situ underwater photographs were collected by snorkelling on 2, 3, and 9 October 2024.

Seven seagrass species have previously been reported from Sepanggar Bay: *E. acoroides* (L.f.) Royle, *C. serrulata* (R.Brown) Ascherson & Magnus, *Cymodocea rotundata*, *Thalassia hemprichii*, *H. ovalis* (R.Brown) Hook.f., *Halodule uninervis*, and *Syringodium isoetifolium* (Bujang et al., 2006). In this study, three targeted species were consistently observed across the port footprint and utilized for the spatial classification modeling: *E. acoroides*, *C. serrulata*, and *H. ovalis*.

The methodological workflow comprised four steps: (i) collection of in-situ reference photographs for training and validation; (ii) UAV imagery acquisition over the study area; (iii) object-based image analysis (OBIA) and habitat classification using machine learning; and (iv) accuracy assessment of the classified map.

2.2. In-situ data collection

In-situ benthic habitat surveys were conducted to support habitat classification and accuracy assessment. A total of 629 in-situ reference points were collected across the study area.

In-situ reference data were collected by snorkelling and consisted of geo-referenced underwater photographs used to define the habitat classification scheme and support map validation. Photographs were captured using a GoPro Hero 11 Black and an Olympus TG6 underwater camera, while a Garmin 64S handheld GPS (attached to the snorkeller's life jacket) recorded the survey track to support georeferencing of observations.

At each survey location, benthic habitat type was identified visually based on dominant substrate and biological cover. Habitat observations were classified into six benthic habitat classes: seagrass (SG), mixed seagrass (MSG), coral (C), deep water (DW), fine sand (FS), and coral rubble and coarse sand (CR) (Fig. 3; Table 1). Seagrass species identification was conducted in-situ based on macro-morphological characteristics observed in the field—including leaf blade width, apical margin serration, sheath structures, and rhizome configurations. To ensure taxonomic accuracy and methodological reproducibility, identification was systematically cross-referenced with standard regional taxonomic keys for the Indo-West Pacific (Kuo and Hartog, 2001; Waycott et al., 2004), as well as established localized identification criteria for Malaysian coastal waters (Bujang et al., 2006). The targeted species identified within the port footprint were *E. acoroides* (L.f.) Royle, *H. ovalis* (R.Brown) Hook.f., and *C. serrulata* (R.Brown) Ascherson & Magnus (synonym: *Oceana serrulata*), with the latter recorded under its currently accepted binomial designation in accordance with the World

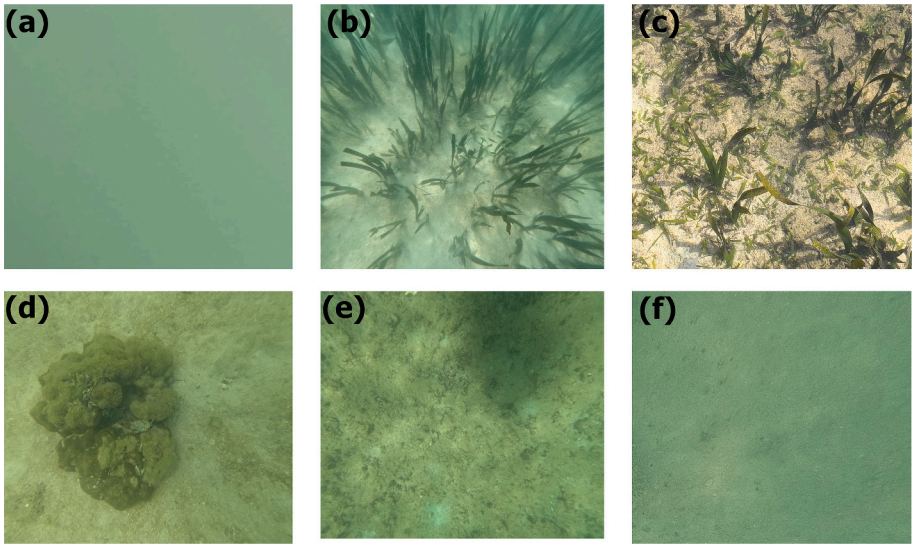

Fig. 3. Representative underwater photographs of benthic habitat classes identified during in situ validation surveys: (a) deep water (DW); (b) seagrass (SG) meadow dominated by *E. acoroides*; (c) mixed seagrass (MSG) assemblage featuring *C. serrulata*, *H. ovalis*, and *E. acoroides*; (d) massive coral (C) colony; (e) coral rubble and coarse sand (CR); and (f) fine sand (FS) substrate.

Table 1
Benthic habitat classification scheme used for UAV-based mapping and accuracy assessment at Sabah Port.

Code	Classification classes	Description
C	Coral	Massive corals. Dome-shaped, hemispherical, or irregularly boulder-like forms. Usually small (less than 50 cm in diameter) and located near deep water areas (e.g., Sabah Port). The surface appears smooth but may have subtle grooves, ridges, or nodules.
CR	Coral rubble and coarse sand	Fragments of dead coral, mollusc shells, and other hard structures (sizes vary from a few millimetres to several centimetres). Coral rubble and coarse sand typically form large patches distinguishable from fine sand by darker colouration and algae attachment.
DW	Deep water	Water regions deeper than 5 m, consists of patch coral.
MSG	Mixed seagrass	The combination of *E. acoroides, C. serrulata*, and *H. ovalis*. *E. acoroides* dominates the meadows, with *C. serrulata* occasionally visible and *H. ovalis* rarely found in less dense seagrass meadows. *C. serrulata.* Narrow, linear leaves (10–20 cm long, 3–5 mm wide) with serrated edges and rounded or slightly rounded notched tips. Bright green to olive in colour. Creeping, slender rhizomes, and fibrous roots are found in sandy or silty substrates. *H. ovalis.* Short, oval to spoon-shaped leaves (2–6 cm long, 2–6 mm wide) with smooth margins. Light green colour with a soft, delicate texture. Thin rhizomes and fine roots in soft mud or sand.
FS	Fine sand	Fine sand with sediment size 0.063 mm–0.25 mm in diameter. Smooth and soft texture. The colour is often pale in colour (white, beige, or grey), depending on the composition.
SG	Seagrass	*E. acoroides.* Long, ribbon-like, strap-shaped seagrass leaves (50–150 cm in length, 1–2 cm in width). Smooth, leathery texture with rounded and blunt tips. Thick, woody rhizomes. The largest seagrass species in Malaysia is easily visible in drone images.

Register of Marine Species (WoRMS) database. Monospecific and mixed seagrass assemblages were recorded separately. In-situ reference data were subsequently divided into two datasets. A subset of reference points was used for training sample selection during object-based image classification, while the remaining points were reserved for independent accuracy assessment.

Seagrass species identification was based on morphological characteristics observed in the field, including leaf shape, size, and growth form. Monospecific and mixed seagrass assemblages were recorded separately. To maintain strict analytical independence, the 629 collected in situ reference points were designated entirely as an independent validation dataset and were withheld completely from the initial image classification process. These 629 ground-truth points were later used exclusively to populate the accuracy assessment confusion matrix. The classification scheme used for in situ validation and subsequent UAV image interpretation is summarised in Table 1.

2.3. UAV image acquisition

UAV imagery was acquired on September 20, 2024, at Sabah Port. The UAV survey used a DJI Mavic 2 Pro equipped with a Hasselblad L1D-20c camera. The sensor recorded imagery in the visible range (approximately 400–700 nm; RGB). The UAV survey covered a total area of 9.364 ha and was conducted in three flight missions to ensure complete coverage and operational safety.

Flight missions were planned using the Litchi Mission Hub (v4.0.1; https://flylitchi.com/hub) (Fig. 4). The UAV was flown at an altitude of 52.2 m above ground level (AGL) at a ground speed of 5 m s^{-1}. Image acquisition was configured with 70% forward and 70% side overlaps. The camera gimbal was oriented nadir (90°) throughout the acquisition. Each mission lasted approximately 15 min (approximately 45 min in total). Flights were conducted in the early morning during low tide to minimise sun glint and maximise water column visibility. The UAV mission was authorised by the Civil Aviation Authority of Malaysia (CAAM/BOP/ATF/P2024/09/2490).

2.4. Image pre-processing and orthomosaic generation

UAV imagery was processed using a structure-from-motion (SfM) photogrammetry workflow to generate a georeferenced orthomosaic of the study area. Image geolocation was based on onboard GNSS geotags. The output products were generated in the WGS84 coordinate system (EPSG:4326). A total of 755 images acquired during the three flight missions were used for reconstruction. Photogrammetric processing was performed using Agisoft Metashape Professional (v2.0.4; https://www.

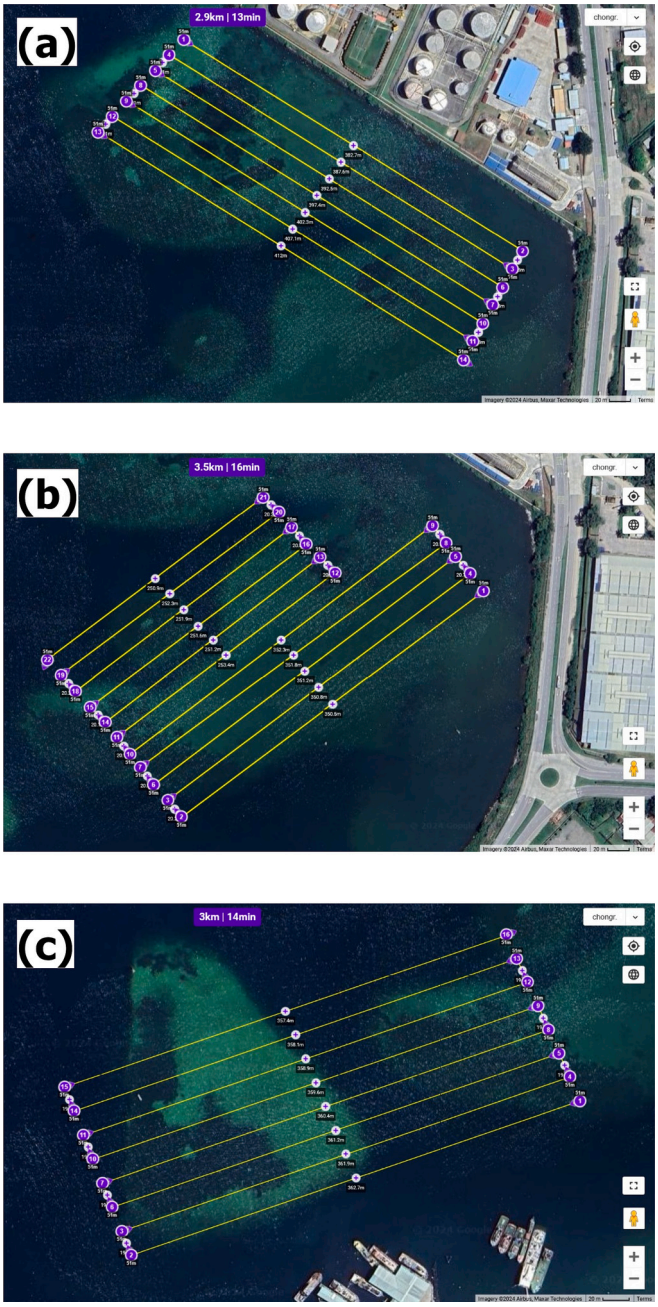

Fig. 4. Planned UAV flight paths covering the study area at the Sabah Port.

agisoft.com/). Images were aligned to build a sparse point cloud, followed by dense point cloud generation, mesh reconstruction, texture generation, and orthomosaic export. Processing settings were: alignment accuracy High; generic preselection Yes; reference preselection Source; key point limit 40,000 (1000 per Mpx); tie point limit 4000; exclude stationary tie points Yes; depth map quality Medium; filtering mode Mild; maximum neighbours 16.

The resulting dense point cloud contained 56,657,606 points in total. The reconstructed mesh comprised 3,643,490 faces and 1,822,367 vertices with a texture size of 8192 × 8192. The exported orthomosaic measured 51,053 × 42,177 pixels with mosaic blending and hole filling enabled. The final orthomosaic was exported for OBIA processing.

2.5. Object-based image analysis and habitat classification

Benthic habitat classification was conducted using an OBIA approach (Blaschke, 2010; Price et al., 2022). The UAV orthomosaic was segmented using multiresolution segmentation to delineate image objects with internally homogeneous spectral properties (Fig. 5). The segmentation parameters were selected through iterative testing; the final settings were a scale parameter of 50, shape 0.1, and compactness 0.8 in Trimble eCognition software (v10.4; https://geospatial.trimble.com/en).

After segmentation, a support vector machine (SVM) classifier was trained. Training samples were selected using an on-screen purposive sampling strategy within Trimble eCognition software, where a human operator digitised homogenous seed-objects representing clear examples of each habitat class (CR, C, FS, DW, SG, and MSG) across the orthomosaic. This visual selection was guided by field photo-keys and localized site familiarity, ensuring that training objects were structurally distinct and spatially disconnected from the 629 independent validation points to avoid spatial autocorrelation or data-leakage. The trained SVM model was then used to classify all image objects across the orthomosaic. Post-classification refinement was undertaken to reduce obvious artifacts and localized misclassification, particularly along class boundaries and transition zones.

To quantify habitat area, the classified raster was exported as a GeoTIFF and analysed using class statistics. Class areas were calculated by multiplying the number of pixels per class by the pixel ground area derived from the orthomosaic spatial resolution, and the results were converted to hectares for reporting (Carpenter et al., 2022).

2.6. Accuracy assessment

Classification accuracy was evaluated using independent in-situ reference data. An error (confusion) matrix was constructed to summarise the agreement between the mapped and reference classes and to compute the overall accuracy (OA), producer accuracy (PA), and user accuracy (UA) for each benthic habitat class (Congalton and Green, 2013).

Agreement beyond chance was quantified using the Kappa coefficient (κ), which accounts for agreement expected by chance based on the marginal totals of the error matrix (Tang et al., 2015). The Tau coefficient (τ) was also calculated as a chance-corrected agreement measure under an equal-probability assumption across classes, expressed as $\tau = (P_o - 1/k)/(1-1/k)$, where P_o is the observed proportion agreement and k is the number of classes.

3. Results

3.1. Spatial distribution of benthic habitats and seagrass

The UAV survey produced a seamless orthomosaic with a spatial resolution of 1.31 cm per pixel, enabling centimetre-scale delineation of shallow-water habitat heterogeneity across the 9.364 ha study area at Sabah Port, Sepanggar Bay (Fig. 6). At this spatial scale, substrate texture (e.g. fine sand versus coral rubble) and patchy vegetation cover were visually distinguishable, particularly in the nearshore zones.

OBIA delineated six benthic habitat classes: SG, MSG, C, CR, FS, and DW (Fig. 7). FS was the dominant class (3.819 ha; ~41%), followed by CR (3.597 ha; ~39%) and DW (1.139 ha; ~12%), respectively. C occupied 0.287 ha (~3%), reflecting the predominantly sediment-dominated nature of the port environment.

Seagrass habitats (SG and MSG) covered 0.522 ha (~6% of mapped area). The SG class (0.304 ha; ~3%) represented dense meadows dominated by *E. acoroides*, while MSG (0.218 ha; ~2%) corresponded to mixed assemblages in which *C. serrulata* and *H. ovalis* co-occurred with *E. acoroides* patches (Fig. 8). Seagrass occurrence decreased with increasing water depth and distance from the shoreline, with the deepest sectors classified predominantly as DW and were largely devoid of vegetation.

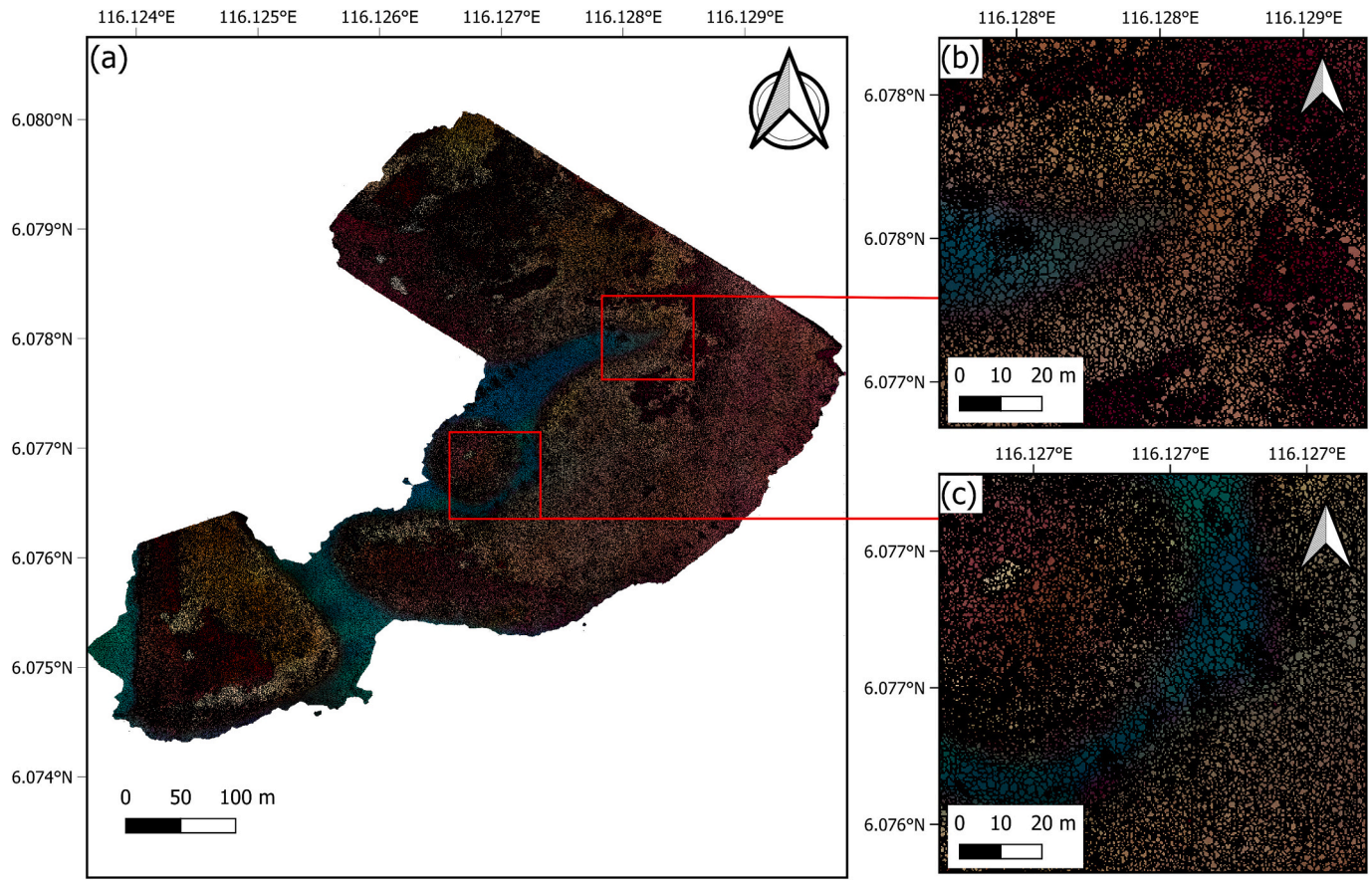

Fig. 5. Segmented UAV orthomosaic used for object-based image analysis.

3.2. Classification accuracy and error characteristics

The OBIA classification achieved an overall accuracy of 88.71% (558 correctly classified out of 629 validation samples), with a Kappa coefficient of 0.843 and a Tau coefficient of 0.865 (Table 2).

Substrate-dominated classes were mapped with high reliability. FS and C classes achieved 100% user accuracy, while CR also showed high user accuracy (95.48%). DW showed high producer accuracy (97.65%) but lower user accuracy (80.58%), indicating confusion at depth-transition boundaries where shallow substrates and deeper water were spectrally similar in RGB imagery. The largest errors were associated with vegetation classes: user accuracy was 48.28% for SG and 50.00% for MSG. Misclassification occurred primarily between SG and MSG, as well as between the seagrass categories and adjacent substrate classes, notably CR and FS.

4. Discussion

The classified map shows that benthic habitats at Sabah Port are dominated by FS (3.819 ha; ~41%) and CR (3.597 ha; ~39%), comprising most of the mapped area. DW covered 1.139 ha (~12%), while C occupied 0.287 ha (~3%). Seagrass habitats (SG and MSG) covered 0.522 ha (~6%) of the 9.364 ha study area and were concentrated in shallow nearshore zones. Dense monospecific meadows dominated by *E. acoroides* accounted for 0.304 ha (~3%), while mixed assemblages (0.218 ha; ~2%) occurred mainly along meadow margins and transition zones. This nearshore distribution aligns with reported seagrass occurrence and sensitivity to coastal development in Sabah (Bujang et al., 2006).

Substrate conditions and functional life-history traits likely contributed to the spatial dominance of *E. acoroides*. Under the established functional framework for global seagrass ecological strategies, *E. acoroides* is categorized as a long-lived, "persistent" climax species characterized by high physiological resistance to environmental stress, massive anchoring root architectures, large carbohydrate reserves in woody rhizomes, and slow leaf turnover rates (Kilminster et al., 2015; Orth et al., 2006). These persistent life-history traits enable *E. acoroides* seedlings and mature rhizomes to successfully anchor and persist in coarser, high-energy sediments under localized hydrodynamic exposure or severe vessel-induced wave action within port boundaries (Ambo-Rappe, 2022; van Katwijk and Hermus, 2000). Conversely, mixed assemblages containing *C. serrulata* and *H. ovalis* reflect "opportunistic" or "pioneering" strategies; these species possess rapid growth and high colonization capacities but have low resistance to sediment shifting and burial, restricting them to highly variable, transient boundary zones where canopy density fluctuates at the centimetre scale (Kilminster et al., 2015).

The object-based classification showed high agreement with independent reference data (OA = 88.71%; $\kappa = 0.843$; $\tau = 0.865$), indicating that UAV RGB imagery can support reliable benthic habitat mapping in a port environment when acquisition conditions are favourable. This high overall classification performance is strongly consistent with previous marine applications that paired object-based image analysis (OBIA) with supervised machine learning algorithms, which consistently outperform traditional pixel-based methods in complex coastal zones by minimizing "salt-and-pepper" noise (Ventura et al., 2018; Wicaksono et al., 2019). For example, (Ventura et al., 2018) achieved an overall accuracy of 89.6% when mapping heterogeneous Mediterranean shallow habitats, which mirrors the 88.71% accuracy achieved in this study. However, notable discrepancies emerge when evaluating individual vegetation class accuracies. Our lower user and producer accuracies for the seagrass classes (48.28% for SG and 50.00% for MSG) represent a documented

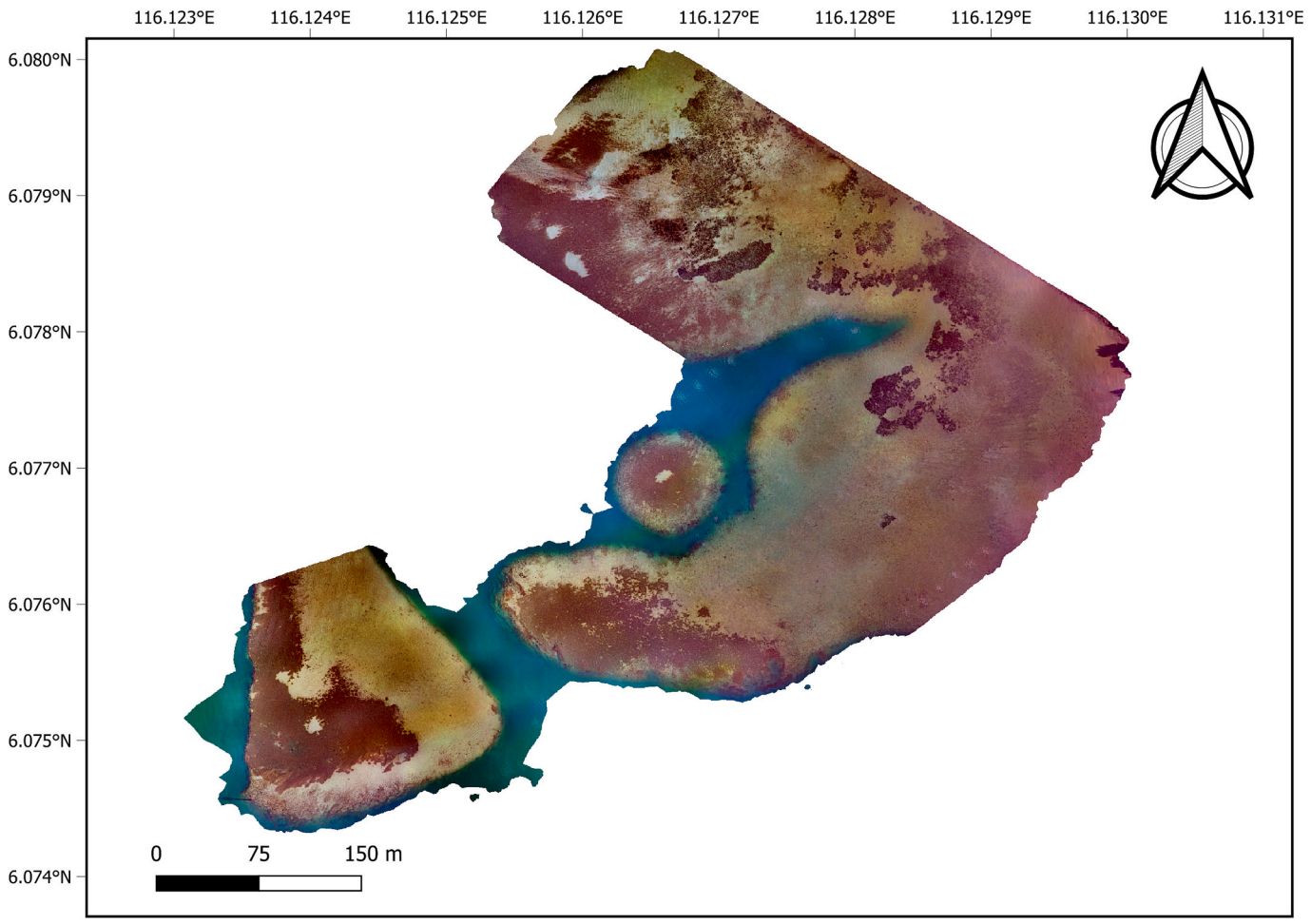

Fig. 6. UAV-derived orthomosaic of the study area at a spatial resolution of 1.31 cm.

challenge shared across coastal remote sensing literature. Similar individual class drops were reported by (Hamad et al., 2022) in Zanzibar and (Duffy et al., 2018) in Western Europe, where standard consumer-grade RGB sensors struggled to separate sparse, low-canopy mixed vegetation from highly reflective sandy backgrounds. While some studies circumvented this by using specialized multispectral sensors to leverage the near-infrared (NIR) bands for sharper vegetation contrast (Duffy et al., 2018), our study demonstrates that an affordable, visible-band RGB drone can still achieve highly comparable spatial definitions for overall habitat boundaries. The specific misclassifications observed between our SG and MSG classes, as well as confusion with surrounding sandy substrates, are consistent with the limits documented by (Wicaksono et al., 2019), who noted that standard visible-band sensors struggle to decouple intermediate pixel signatures caused by spatially patchy canopy cover and mixed substrate backgrounds in shallow-water meadows. Furthermore, unlike the vast majority of prior drone investigations that were conducted within highly transparent marine protected areas or calm, enclosed lagoons (Bremner et al., 2023; Hamad et al., 2022), our workflow was subjected to an active industrial port setting. The structural confusion observed along our deep-water gradients matches the depth-attenuation limits documented by (Trinh et al., 2023) in turbid Vietnamese waters, confirming that water column interference remains a primary operational constraint regardless of whether satellite or ultra-high-resolution drone platforms are deployed.

The lower individual user accuracies observed for the seagrass categories (48.28% for SG and 50.00% for MSG) directly reflect the high spectral and structural overlap inherent to shallow-water mixed meadows when captured using standard visible-band RGB sensors. In heterogeneous port environments, small patch sizes and transitional canopy edges create intermediate pixel values that confuse the machine learning classifiers. Despite these constraints, separating monospecific *E. acoroides* (SG) from mixed *C. serrulata/H. ovalis* assemblages (MSG) was maintained as a deliberate mapping priority. These classes represent fundamentally distinct ecological indicators. *E. acoroides* serves as a highly stable, deep-rooted climax species that binds heavy sand-rubble matrices near industrial boundaries, whereas mixed assemblages represent highly dynamic, low-canopy pioneering stands sensitive to acute dredging impacts and vessel-induced turbidity. To evaluate the underlying reliability of our object-based workflow independent of this subtle biological boundary, a simulated pool of the two categories into a single, unified “Seagrass” class was performed. This simplification eliminated transitional edge-confusion, elevated the overall map accuracy to 89.51%, and increased the unified seagrass user accuracy to 62.2%. This diagnostic step proves that the classification framework retains high spatial fidelity for overall vegetation detection, while the granular multi-class boundaries, although challenging to map perfectly, provide indispensable qualitative value for local community harvesting and habitat-specific impact assessments within the port footprint.

UAV mapping performance in Sabah Port was strongly influenced by the sea state, turbidity, and sun glint, which represent universal challenges for optical shallow-water remote sensing. In this study, localized turbidity driven by tidal currents and active industrial port runoff acted as a primary constraint, as suspended particulate matter restricted downwelling light penetration, thereby reducing the spectral contrast of submerged features and obscuring the deep-water transition zones. Sun glint was structurally mitigated by constraining all three UAV flight

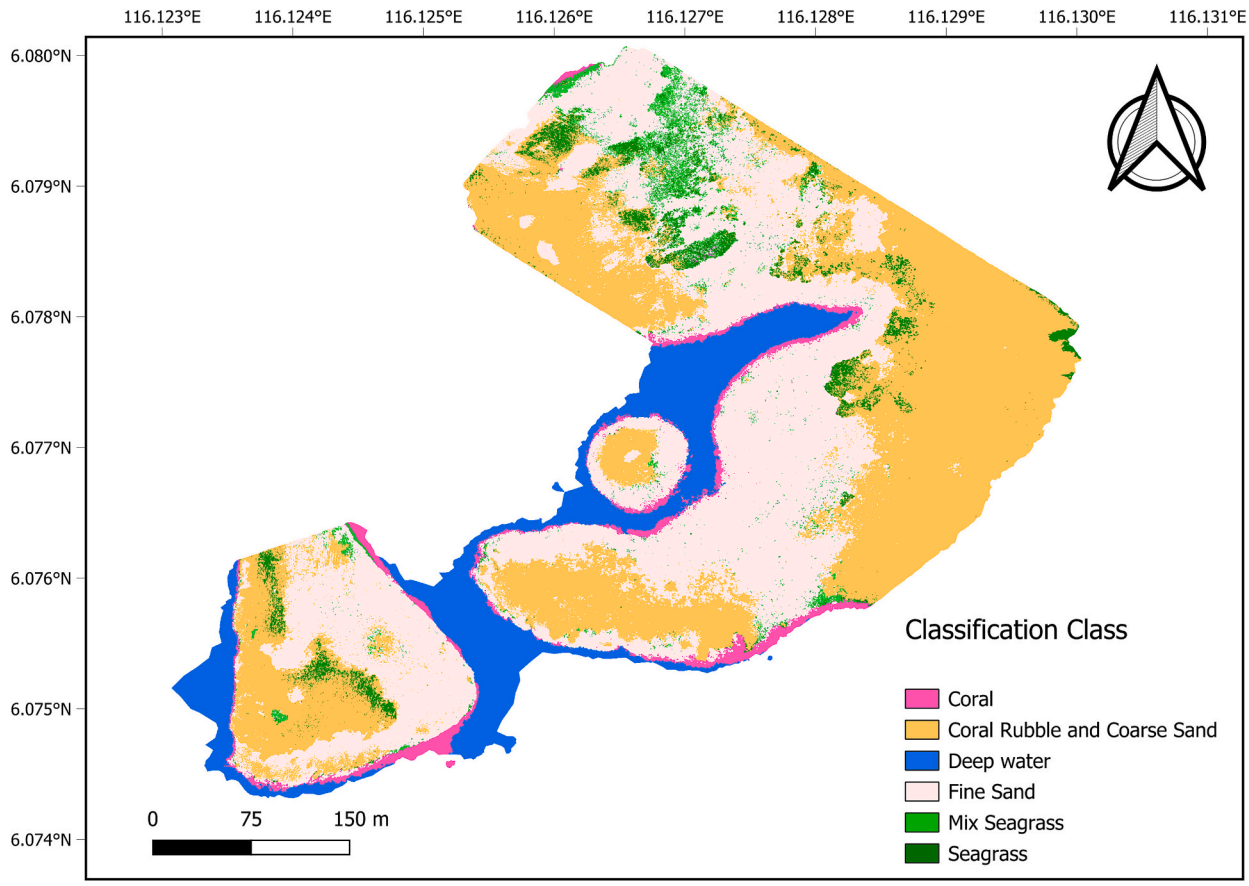

Fig. 7. High-resolution benthic habitat classification map of the Sabah Port derived from UAV imagery.

missions to the early morning hours (between 08:00 and 09:30 local time), avoiding peak midday solar positions to minimise intense specular reflection into the nadir-oriented camera sensor, matching the established survey timing recommendations (Muslim et al., 2019; Qu, 2018). Furthermore, surveys were executed exclusively during a calm sea state corresponding to Beaufort Scale 1–2 (wind speeds <3.3 ms^{-1}) to minimise surface capillary waves that induce geometric distortions during photogrammetric SfM reconstruction. Despite these flight planning constraints, residual environmental artifacts persisted; localized surface ripples and white water generated by the hulls of passing commercial container vessels created isolated patches of high surface reflectance. These surface reflections and increased sediment resuspension degraded orthomosaic quality and increased classification uncertainty in shallow coastal settings (Chong et al., 2023), particularly where sparse vegetation boundaries met unconsolidated substrates. These operational constraints highlight that achieving repeatable baselines in busy port environments requires standardized, narrow environmental windows that synchronize low tide, low solar glint, and low-traffic calm sea states.

While our workflow demonstrates the operational value of ultra-high-resolution mapping in an industrial landscape, a comprehensive evaluation requires an explicit examination of the economic, personnel, and accuracy limitations inherent to this UAV methodology.

- **Economic Limitations:** Although consumer-grade RGB UAV hardware is highly cost-effective compared to commercial satellite tasking or vessel-based acoustics, the financial barrier shifts significantly to the data processing phase. Reconstructing 755 high-resolution aerial frames requires high-performance computing architecture, costly proprietary structure-from-motion (SfM) photogrammetry software licenses, and advanced object-based image analysis (OBIA) development packages. Additionally, executing commercial-grade monitoring in active logistics zones incurs recurring financial overheads for civil aviation processing fees and liability insurance required to secure legal flight authorizations.
- **Personnel and Expertise Barriers:** The execution of this methodology depends on an interdisciplinary skill set that limits widespread institutional adoption by coastal management agencies. Field personnel must possess formal pilot accreditation to navigate complex aeronautical regulations near industrial infrastructure, while data analysts require specialized training in photogrammetric error optimization, multiresolution segmentation tuning, and machine learning classification workflows. Without this technical expertise, user-defined bias during segmentation or training object selection can severely compromise map reproducibility.
- **Accuracy Constraints:** Radiometrically, the reliance on a standard 3-band visible RGB sensor means the classification accuracy remains highly vulnerable to depth-gradient attenuation and spectral mixing. This constraint is clearly reflected in our lower user accuracies for the individual vegetation categories (48.28% for SG and 50.00% for MSG), where the lack of a near-infrared (NIR) channel prevented the sharp decoupling of low-canopy pioneering stands from highly reflective, unconsolidated sandy and rubble matrices.

Acknowledging these limitations is critical; however, despite these constraints, the workflow's capacity to resolve site-scale baseline configurations within a compressed operational window establishes it as a highly valuable tool for targeted port-scale impact assessments.

The mapped habitat distribution provides baseline spatial information for port-scale environmental assessment and routine monitoring of nearshore habitats. The primary contribution is a validated baseline layer that can be used to track habitat change associated with coastal

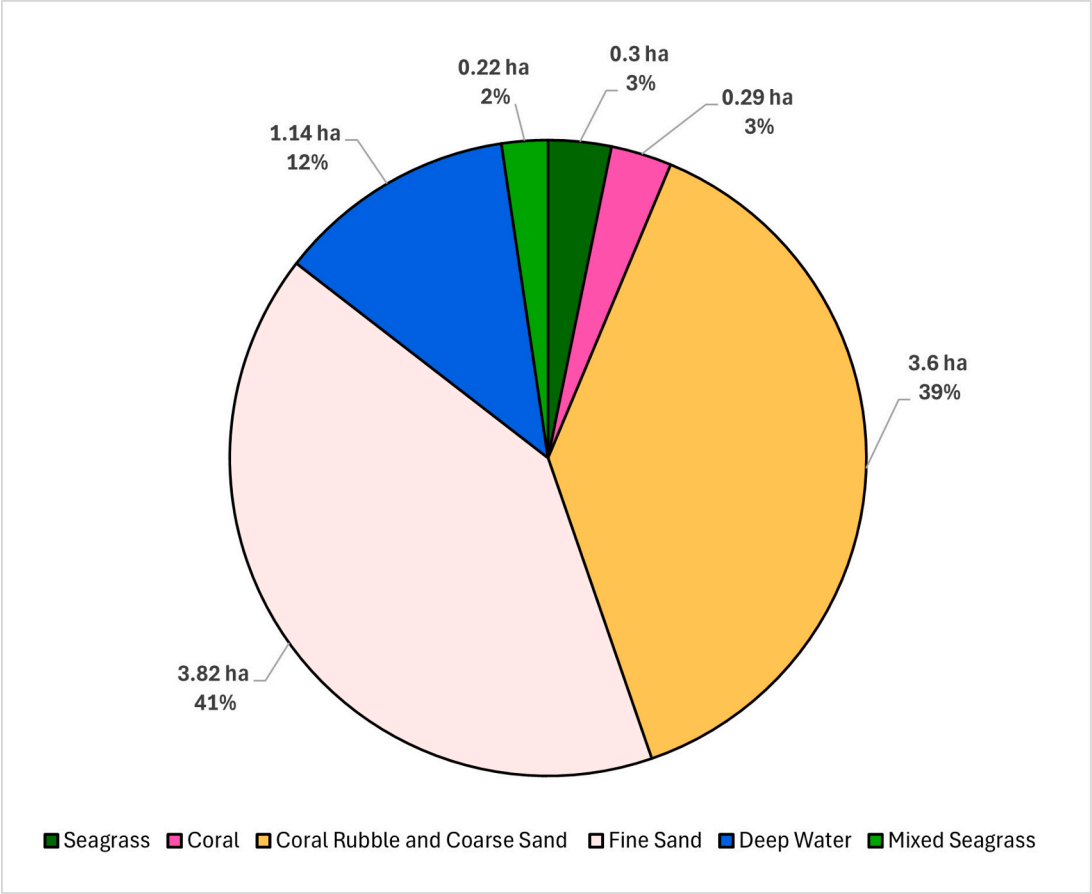

Fig. 8. Relative area coverage of the benthic habitat classes within the study area.

Table 2
Confusion matrix and accuracy metrics for UAV-derived benthic habitat classification.

Classified	Reference								User accuracy (%)
	Code	CR	C	FS	DW	MSG	SG	Row total	
Coral rubble and coarse sand	CR	169	3	0	3	0	2	177	95.48
Coral	C	0	2	0	0	0	0	2	100
Fine sand	FS	0	0	199	0	0	0	199	100
Deep water	DW	7	6	3	166	6	18	206	80.58
Mixed seagrass	MSG	2	2	0	1	8	3	16	50
Seagrass	SG	13	0	0	0	2	14	29	48.28
Producer Accuracy (%)		88.48	15.38	98.51	97.65	50.00	37.84	629	
Number of correctly classified sites	558								
Overall Accuracy (%)	88.712								
Kappa Coefficient (κ)	0.843								
Tau Coefficient (τ)	0.865								

development, dredging activities and sediment dynamics within working ports. Residual confusion between SG and MSG reflects ecological gradients rather than segmentation alone. Mixed assemblages typically occur as patchy mosaics with variable canopy density and exposed substrate, producing intermediate spectral and textural signatures that overlap with dense monospecific meadows. Similar limitations have been reported for object-based benthic habitat classification in optically complex environments (Esetlili et al., 2018; Hue et al., 2026).

Transferability of the workflow depends primarily on acquisition conditions and validation design rather than on site-specific tuning. For regional applications, repeat surveys should standardise tide window, sun angle and sea-state, and maintain consistent class definitions and reference sampling to support comparable time-series mapping.

Repeat UAV surveys can support change detection for seagrass extent and fragmentation at spatial scales relevant to local management. UAV mapping does not replace satellite monitoring, but it is suitable for targeted assessments in spatially complex areas where satellites underperform due to mixed pixels and limited spatial resolution (Ellis et al., 2021; Goodwin et al., 2023).

Operationally, UAV surveys can be completed rapidly without vessel-based sampling in very shallow areas, improving access to nearshore habitats and enabling flexible scheduling (Ventura et al., 2016). These attributes support the use of UAV-derived products as decision-support layers for zoning, baseline documentation, and targeted monitoring in development-pressured coastal settings.

5. Conclusions

This study demonstrates that integrating consumer-grade RGB UAV imagery with an object-based image analysis (OBIA) framework can successfully map nearshore benthic environments within active industrial landscapes, achieving a high overall classification accuracy of 88.71% across a 9.364 ha footprint at Sabah Port. Our findings establish that while abiotic substrates like fine sand and coral rubble dominate the port's shallow footprint, the framework successfully delineates 0.522 ha of critical, development-pressured seagrass and mixed seagrass assemblages concentrated along the shallow coastal fringe.

However, the operational reliability of this visible-band remote sensing pipeline remains constrained by light attenuation across steep depth gradients, localized turbidity spikes from port runoff, and spectral confusion within low-canopy mixed vegetation zones. To overcome these accuracy and radiometric bottlenecks, future iterations of this methodology should prioritize the integration of lightweight multispectral sensors to leverage near-infrared (NIR) and red-edge bands for sharper vegetation contrast, alongside the deployment of localized water-column correction models.

In terms of immediate application, this high-resolution spatial dataset provides a vital, centimetre-scale environmental baseline that allows port authorities and coastal managers to accurately monitor sensitive ecosystems exposed to active maritime infrastructure development. Moving forward, the standardized, rapid-deployment nature of this workflow offers a highly transferable blueprint for executing repeatable, multi-temporal change detection surveys, enabling local environmental management agencies to shift from reactive damage documentation to proactive, adaptive habitat conservation within high-exposure industrial corridors.

Authors' contribution statement

LPZ and CWS conceived the study and designed the methodology. AL, IN, and LPZ conducted field data collection. IN and LPZ performed data analysis. LPZ and CWS led the writing of the manuscript. All authors contributed critically to manuscript revisions and approved the final version for publication.

CRediT authorship contribution statement

Pei Zhao Liew: Writing – review & editing, Writing – original draft, Visualization, Methodology, Investigation, Formal analysis, Conceptualization. **Imelus Nius:** Visualization, Validation, Methodology, Investigation, Formal analysis, Data curation, Conceptualization. **Ashley Loduni:** Writing – original draft, Methodology, Investigation, Formal analysis, Data curation, Conceptualization. **Wei Sheng Chong:** Writing – review & editing, Writing – original draft, Validation, Supervision, Software, Resources, Project administration, Investigation, Funding acquisition.

Declaration of competing interest

The authors declare that they have no known competing financial interests or personal relationships that could have appeared to influence the work reported in this paper.

Acknowledgements

The authors are grateful for the research permit granted by the Sabah Biodiversity Centre (SaBC) with Licence Ref. No. JKM/MBS.100-2/13JLD.2(74), and the Permit of Authorisation to Fly (ATF) for Unmanned Aircraft System (UAS) issued by the Civil Aviation Authority of Malaysia (CAAM) with permit no. CAAM/BOP/ATF/P2024/09/2490. This research was supported by Yayasan PETRONAS for the 'Seagrass Mapping and Community-Based Programme in Sabah and the Federal Territory of Labuan (LKS 2508)'.

Data availability

The authors do not have permission to share data.

References

Ambo-Rappe, R., 2022. The success of seagrass restoration using *Enhalus acoroides* seeds is correlated with substrate and hydrodynamic conditions. J. Environ. Manag. 310, 114692. https://doi.org/10.1016/j.jenvman.2022.114692.

Blaschke, T., 2010. Object based image analysis for remote sensing. ISPRS J. Photogramm. Remote Sens. 65 (1), 2–16. https://doi.org/10.1016/j.isprsjprs.2009.06.004.

Bremner, J., Petus, C., Dolphin, T., Hawes, J., Beguet, B., Devlin, M.J., 2023. A seagrass mapping toolbox for South Pacific environments. Remote Sens. 15 (3). https://doi.org/10.3390/rs15030834.

Bujang, J.S., Zakaria, M.H., Arshad, A., 2006. Distribution and significance of seagrass ecosystems in Malaysia. Aquat. Ecosyst. Health Manag. 9 (2), 203–214. https://doi.org/10.1080/14634980600705576.

Carpenter, S., Byfield, V., Felgate, S.L., Price, D.M., Andrade, V., Cobb, E., Strong, J., Lichtschlag, A., Brittain, H., Barry, C., Fitch, A., Young, A., Sanders, R., Evans, C., 2022. Using unoccupied aerial vehicles (UAVs) to map seagrass cover from Sentinel-2 imagery. Remote Sens. 14 (3), 477. https://doi.org/10.3390/rs14030477.

Chong, W.S., Akmal, K.F., Shah, M.D., 2023. The synergy of remote sensing in marine invasion science. In: Shah, M.D., Ransangan, J., Venmathi Maran, B.A. (Eds.), Marine Biotechnology: Applications in Food, Drugs and Energy. Springer Nature Singapore, pp. 299–313. https://doi.org/10.1007/978-981-99-0624-6_14.

Christianen, M.J.A., van Belzen, J., Herman, P.M.J., van Katwijk, M.M., Lamers, L.P.M., van Leent, P.J.M., Bouma, T.J., 2013. Low-canopy seagrass beds still provide important coastal protection services. PLoS One 8 (5), e62413. https://doi.org/10.1371/journal.pone.0062413.

Congalton, R.G., Green, K., 2013. Assessing the Accuracy of Remotely Sensed Data Principles and Practices, Second edition. CRC Press Taylor & Francis Group, Boca Raton, London, New York.

de los Santos, C.B., Krause-Jensen, D., Alcoverro, T., Marbà, N., Duarte, C.M., van Katwijk, M.M., Pérez, M., Romero, J., Sánchez-Lizaso, J.L., Roca, G., Jankowska, E., Pérez-Lloréns, J.L., Fournier, J., Montefalcone, M., Pergent, G., Ruiz, J.M., Cabaço, S., Cook, K., Wilkes, R.J., Santos, R., 2019. Recent trend reversal for declining European seagrass meadows. Nat. Commun. 10 (1), 3356. https://doi.org/10.1038/s41467-019-11340-4.

Duffy, J.P., Pratt, L., Anderson, K., Land, P.E., Shutler, J.D., 2018. Spatial assessment of intertidal seagrass meadows using optical imaging systems and a lightweight drone. Estuar. Coast. Shelf Sci. 200, 169–180. https://doi.org/10.1016/j.ecss.2017.11.001.

Ellis, S.L., Taylor, M.L., Schiele, M., Letessier, T.B., 2021. Influence of altitude on tropical marine habitat classification using imagery from fixed-wing, water-landing UAVs. Remote Sens. Ecol. Conserv. 7 (1), 50–63. https://doi.org/10.1002/rse2.160.

Esetlili, Mt., Balcik, F.B., Şanlı, F.B., Üstüner, M., Kalkan, K., Göksel, Ç., Gazioğlu, C., Kurucu, Y., Aksu, A., Alpar, B., Altuğ, G., Balas, L., Balas, C., Bat, L., Bayram, B., Çağlar, N., Dash, J., Erginal, A.E., Fritsch, D., Zeki, S., 2018. Comparison of object and pixel-based classifications for mapping crops using Rapideye imagery: a case study of Menemen plain, Turkey. Int. J. Environ. Geoinform. 5 (2), 231–243. https://doi.org/10.30897/ijegeo.

Fortes, M.D., Ooi, J.L.S., Tan, Y.M., Prathep, A., Bujang, J.S., Yaakub, S.M., 2018. Seagrass in Southeast Asia: a review of status and knowledge gaps, and a road map for conservation. Bot. Mar. 61 (3), 269–288. https://doi.org/10.1515/bot-2018-0008.

Freeman, A.S., Short, F.T., Isnain, I., Razak, F.A., Coles, R.G., 2008. Seagrass on the edge: land-use practices threaten coastal seagrass communities in Sabah, Malaysia. Biol. Conserv. 141 (12), 2993–3005. https://doi.org/10.1016/j.biocon.2008.09.018.

Goodwin, G., Marani, M., Silvestri, S., Carniello, L., Alpaos, A. D. (2023). Toward Coherent Space-Time Mapping of Seagrass Cover from Satellite Data: Example of a Mediterranean Lagoon. doi:https://doi.org/10.5194/egusphere-2022-1501.

Greene, A., Rahman, A.F., Kline, R., Rahman, M.S., 2018. Side scan sonar: a cost-efficient alternative method for measuring seagrass cover in shallow environments. Estuar. Coast. Shelf Sci. 207, 250–258. https://doi.org/10.1016/j.ecss.2018.04.017.

Hamad, I.Y., Staehr, P.A., Rasmussen, M.B., Sheikh, M., 2022. Drone-based characterization of seagrass habitats in the tropical waters of Zanzibar. Remote Sens. 14 (3), 680. https://doi.org/10.3390/rs14030680.

Hossain, M.S., Bujang, J.S., Zakaria, M.H., Hashim, M., 2015, January. The application of remote sensing to seagrass ecosystems: an overview and future research prospects. Int. J. Remote Sens. 36 (1), 61–114. Taylor and Francis Ltd. https://doi.org/10.1080/01431161.2014.990649.

Hue, C., Chong, W.S., Rasib, A.W., Tang, K.K.W., 2026. Elucidating the potential of unmanned aerial vehicle (UAV) and satellite imagery for the improvement of coral reef community mapping. Int. J. Remote Sens. 1–36. https://doi.org/10.1080/01431161.2026.2680711.

Kamal, A.H.M., Al-Asif, A., Idris, M.H., Bhuiyan, M.K.A., Rahman, A., 2023. Trends in Seagrass Research and Conservation in Malaysian Waters.

Kilminster, K., McMahon, K., Waycott, M., Kendrick, G.A., Scanes, P., McKenzie, L., O'Brien, K.R., Lyons, M., Ferguson, A., Maxwell, P., Glasby, T., Udy, J., 2015. Unravelling complexity in seagrass systems for management: Australia as a microcosm. Catalysing transdisciplinary synthesis in ecosystem science and

management. Sci. Total Environ. 534, 97–109. https://doi.org/10.1016/j.scitotenv.2015.04.061.
Koedsin, W., Intararuang, W., Ritchie, R., Huete, A., 2016. An integrated field and remote sensing method for mapping seagrass species, cover, and biomass in southern Thailand. Remote Sens. 8 (4), 292. https://doi.org/10.3390/rs8040292.
Kuo, J., Hartog, C., 2001. Seagrass taxonomy and identification key. In: Global Seagrass Research Methods, pp. 31–58. https://doi.org/10.1016/B978-044450891-1/50003-7.
Lin, J., Liu, X., Lai, T., He, B., Du, J., Zheng, X., 2021. Trophic importance of the seagrass *Halophila ovalis* in the food web of a Hepu seagrass bed and adjacent waters, Beihai, China. Ecol. Indic. 125, 107607. https://doi.org/10.1016/j.ecolind.2021.107607.
Makri, D., Melillos, G., Kalogirou, E., Hadjimitsis, D., 2023. Seagrass mapping in Cyprus area of interest with pixel-based classification. In: Hou, W., Mullen, L.J. (Eds.), Ocean Sensing and Monitoring, XV. SPIE, p. 19. https://doi.org/10.1117/12.2663484.
Muhamad, M.A.H., Hasan, R.C., Said, N.M., Ooi, J.L.-S., 2021. Seagrass habitat suitability model for Redang Marine Park using multibeam echosounder data: testing different spatial resolutions and analysis window sizes. PLoS One 16 (9), e0257761. https://doi.org/10.1371/journal.pone.0257761.
Muslim, A.M., Chong, W.S., Safuan, C.D.M., Khalil, I., Hossain, M.S., 2019. Coral reef mapping of UAV: a comparison of sun glint correction methods. Remote Sens. 11 (20), 2422. https://doi.org/10.3390/rs11202422.
Orth, R.J., Heck Jr., K.L., 2023. The dynamics of seagrass ecosystems: history, past accomplishments, and future prospects. Estuar. Coasts 46 (7), 1653–1676. https://doi.org/10.1007/s12237-023-01252-4.
Orth, R.J., Carruthers, T.J.B., Dennison, W.C., Duarte, C.M., Fourqurean, J.W., Heck, K. L., Hughes, A.R., Kendrick, G.A., Kenworthy, W.J., Olyarnik, S., Short, F.T., Waycott, M., Williams, S.L., 2006. A global crisis for seagrass ecosystems. BioScience 56 (12), 987–996. https://doi.org/10.1641/0006-3568(2006)56%5B987:AGCFSE%5D2.0.CO;2.
Price, D.M., Felgate, S.L., Huvenne, V.A.I., Strong, J., Carpenter, S., Barry, C., Lichtschlag, A., Sanders, R., Carrias, A., Young, A., Andrade, V., Cobb, E., Bas, T.L., Brittain, H., Evans, C., 2022. Quantifying the intra-habitat variation of seagrass beds with unoccupied aerial vehicles (UAVs). Remote Sens. 14 (3), 480. https://doi.org/10.3390/rs14030480.
Qu, Y., 2018. Sea surface albedo. In: Comprehensive Remote Sensing. Elsevier, pp. 163–185. https://doi.org/10.1016/B978-0-12-409548-9.10371-9.
Rahman, S.A., Yaakub, S.M., 2020. Socio-economic valuation of seagrass meadows in the Pulai River estuary, peninsular Malaysia, through a wellbeing lens. Mar. Freshw. Res. 71 (8), 877–891. https://doi.org/10.1071/MF19208.
Rajamani, L., Marsh, H., 2015. Mapping seagrass cost-effectively in the coral triangle: Sabah, Malaysia as a case study. Pac. Conserv. Biol. 21 (2), 113. https://doi.org/10.1071/PC14908.
Román, S., Olabarria, C., Román, M., Vázquez, E., 2024. Recovery of fishery-stressed seagrass meadows is driven by improvements in wastewater management. Mar. Pollut. Bull. 201, 116282. https://doi.org/10.1016/j.marpolbul.2024.116282.
Tahara, S., Sudo, K., Yamakita, T., Nakaoka, M., 2022. Species level mapping of a seagrass bed using an unmanned aerial vehicle and deep learning technique. PeerJ 10, e14017. https://doi.org/10.7717/peerj.14017.
Tan, Y.M., Dalby, O., Kendrick, G.A., Statton, J., Sinclair, E.A., Fraser, M.W., Macreadie, P.I., Gillies, C.L., Coleman, R.A., Waycott, M., van Dijk, K., Vergés, A., Ross, J.D., Campbell, M.L., Matheson, F.E., Jackson, E.L., Irving, A.D., Govers, L.L., Connolly, R.M., Sherman, C.D.H., 2020. Seagrass restoration is possible: insights and lessons from Australia and New Zealand. Front. Mar. Sci. 7. https://doi.org/10.3389/fmars.2020.00617.
Tang, W., Hu, J., Zhang, H., Wu, P., He, H., 2015. Kappa coefficient: a popular measure of rater agreement. Shanghai Arch. Psychiatry 27 (1), 62–67. https://doi.org/10.11919/j.issn.1002-0829.215010.
Trinh, X.T., Nguyen, L.D., Takeuchi, W., 2023. Sentinel-2 mapping of a turbid intertidal seagrass meadow in southern Vietnam. Geocarto Int. 38 (1), 2186490. https://doi.org/10.1080/10106049.2023.2186490.
van Katwijk, M., Hermus, D.C.R., 2000. Effects of water dynamics on *Zostera marina*: transplantation experiments in the intertidal Dutch Wadden Sea. Mar. Ecol. Prog. Ser. 208, 107–118. https://doi.org/10.3354/meps208107.
Ventura, D., Bruno, M., Lasinio, G.J., Belluscio, A., Ardizzone, G., 2016. A low-cost drone based application for identifying and mapping of coastal fish nursery grounds. Estuar. Coast. Shelf Sci. 171, 85–98. https://doi.org/10.1016/j.ecss.2016.01.030.
Ventura, D., Bonifazi, A., Gravina, M.F., Belluscio, A., Ardizzone, G., 2018. Mapping and classification of ecologically sensitive marine habitats using unmanned aerial vehicle (UAV) imagery and object-based image analysis (OBIA). Remote Sens. 10 (9), 1331. https://doi.org/10.3390/rs10091331.
Waycott, M., McMahon, K., Mellors, J., Calladine, A., Kleine, D., 2004. A Guide to Tropical Seagrasses of the Indo-West Pacific.
Wicaksono, P., Lazuardi, W., 2021. Assessment of planet scope images for benthic habitat and seagrass species mapping in a complex optically shallow water environment. In: Fine Resolution Remote Sensing of Species in Terrestrial and Coastal Ecosystems. Routledge, pp. 143–169. https://doi.org/10.4324/9781003191193-8.
Wicaksono, P., Aryaguna, P.A., Lazuardi, W., 2019. Benthic habitat mapping model and cross validation using machine-learning classification algorithms. Remote Sens. 11 (2), 1–24. https://doi.org/10.3390/rs11111279.
Zakaria, M.H., Syed, N.N.F., Bujang, J.S., 2025a. The vulnerable seagrass *Halophila beccarii* Aschers. (Hydrocharitaceae) from Malaysia. Front. Conserv. Sci. 6. https://www.frontiersin.org/journals/conservation-science/articles/10.3389/fcosc.2025.1648415.
Zakaria, M.H., Syed, N.N.F., Ramaiya, S.D., Bujang, J.S., 2025b. Seagrass assisted recovery and long-term monitoring in the Sungai Pulai estuary, Johor, Malaysia. Front. Conserv. Sci. 6. https://www.frontiersin.org/journals/conservation-science/articles/10.3389/fcosc.2025.1646399.